applied sciences

MDPI

Article

Contribution of Gravity Data for Structural Characterization of the Ifni Inlier, Western Anti-Atlas, Morocco: Hydrogeological Implications

Mustapha Ikirri [1], Mohammed Jaffal [2,3], Ibtissam Rezouki [4], Fatima Zahra Echogdali [1], Said Boutaleb [1], Kamal Abdelrahman [5], Tamer Abu-Alam [6,7,*], Farid Faik [1], Azzouz Kchikach [2,3] and Mohamed Abioui [1,8,*]

1 Department of Earth Sciences, Faculty of Sciences, Ibnou Zohr University, Agadir 80000, Morocco
2 Georesources, Geoenvironment and Civil Engineering Laboratory, Department of Earth Sciences, Faculty of Sciences and Techniques, Cadi Ayyad University, Marrakech 40000, Morocco
3 Geology and Sustainable Mining Institute (GSMI), Mohammed VI Polytechnic University, Benguerir 43150, Morocco
4 Department of Earth Sciences, Faculty of Sciences, Moulay Ismail University, Meknes 11201, Morocco
5 Department of Geology & Geophysics, College of Science, King Saud University, Riyadh 11451, Saudi Arabia
6 The Faculty of Biosciences, Fisheries and Economics, UiT the Arctic University of Norway, 9037 Tromsø, Norway
7 OSEAN—Outermost Regions Sustainable Ecosystem for Entrepreneurship and Innovation, University of Madeira Colégio dos Jesuítas, 9000-039 Funchal, Portugal
8 MARE—Marine and Environmental Sciences Centre—Sedimentary Geology Group, Department of Earth Sciences, Faculty of Sciences and Technology, University of Coimbra, 3030-790 Coimbra, Portugal
* Correspondence: tamer.abu-alam@uit.no (T.A.-A.); m.abioui@uiz.ac.ma (M.A.)

Abstract: The Sidi Ifni region in southwest Morocco is mainly composed of crystalline rocks with limited groundwater storage capacity. These water resources drain in particular fault zones with high fracture permeability. The main objective of this study is to describe the geological structure of the region to optimize future drilling locations. The gravity data were processed using various techniques, such as total horizontal gradient, tilt derivative, and Euler deconvolution, in conjunction with the interpretation of the geological data, to create a new structural map. This map confirms the presence of many previously identified or inferred faults and identifies significant new faults with their respective trends and depths. Analysis of this map shows that major faults are oriented NNE-SSW and NE-SW, while minor faults are oriented E-W, NW-SE, and NNW-SSE. The superposition of the hydrogeological data and the structural map reveals that the high groundwater flow values in the boreholes are located in the vicinity of the major faults and talwegs. The structures deduced from the filtering and interpretation of the gravity data suggest that the hydrogeological system of the Ifni Inlier is controlled by its structures. To confirm this impact, a high-resolution electrical resistivity map (7200 Hz) was used, with penetration depths ranging from 84 to 187 m. Negative boreholes, located in high resistivity ranges corresponding to sound basement formations without fault crossings, showed high resistivity values. The positive holes, located in anomalies with low linear resistivity, revealed the impact of fault crossings, which drain water and tend to decrease the resistivity values of the formations. Therefore, these new structural maps will assist in planning future hydrogeological studies in this area.

Keywords: Ifni inlier; crystalline basement; bouguer anomaly; residual anomaly; total horizontal gradient; Euler deconvolution; groundwater

Citation: Ikirri, M.; Jaffal, M.; Rezouki, I.; Echogdali, F.Z.; Boutaleb, S.; Abdelrahman, K.; Abu-Alam, T.; Faik, F.; Kchikach, A.; Abioui, M. Contribution of Gravity Data for Structural Characterization of the Ifni Inlier, Western Anti-Atlas, Morocco: Hydrogeological Implications. *Appl. Sci.* **2023**, *13*, 6002. https://doi.org/10.3390/app13106002

Academic Editor: Nicholas Vassiliou Sarlis

Received: 14 January 2023
Revised: 28 April 2023
Accepted: 10 May 2023
Published: 13 May 2023

1. Introduction

Morocco experiences a semi-arid climate characterized by low and irregular annual rainfall, usually less than 200 mm per year, high temperatures, and evaporation rates exceeding 1000 mm, particularly in the southern regions [1–3]. This has been exacerbated in

recent decades by recurring droughts, resulting in water scarcity and the depletion of many water sources that are critical for the survival of the population [4]. In the Sidi Ifni region of southwest Morocco, households often face water shortages due to the overexploitation and vulnerability of surface water sources to drought, as well as high rates of evaporation, which exacerbate surface water depletion. Additionally, completed wells in the area have low flow rates and uneven distribution, with 60% showing very low flows (0.5 to 1.2 L/s) and 30% being dehydrated due to the thick geological substratum dominating the area. Most water inflows in these wells coincide with faults or fractures [5–8]. Given these challenges, a comprehensive understanding of the aquifer system in the Ifni inlier is necessary to improve groundwater recognition and exploitation. The research problem addressed in this study is to enhance the structural understanding of the region to rationalize drilling campaigns. To achieve this, the gravimetric method has been used as an indirect technique for mapping geological structures, even in areas concealed by the sedimentary cover. In the hydrogeological context of the Ifni inlier, these structures play a crucial role in the drainage and storage of groundwater, making their mapping and characterization critical. The Ifni inlier, which provides a window into the Precambrian basement of the Anti-Atlas, is composed of crystalline rocks hosting fissured aquifers, where groundwater is contained in tectonic discontinuities such as faults, fractures, and alluvial depressions. To map the tectonic faults and their influence on groundwater dynamics in the Ifni inlier, indirect geophysical methods are needed due to the presence of a thin Quaternary cover obstructing geological observations and surface data [9–15]. This study aims to use gravity data analysis to create a detailed map of the fault systems affecting the study area for hydrogeological reconnaissance purposes [11–15]. The residual gravity data, derived from subtracting the regional anomaly component from the Bouguer anomaly map, is analyzed using different transformation techniques to analyze the gradient of the gravity field [13,16–26]. The Horizontal Gradient filter transforms the inflection point of the residual gravity profile into a positive anomaly whose maximum coincides with the fault location, while the Tilt derivative filter is used to confirm the fault position [26–30]. Finally, the Euler deconvolution is applied to determine the fault depth of rooting [17,28,31–36]. The obtained results are used to establish a comprehensive structural map of the study area, which is analyzed in conjunction with all the available geological, structural, and drilling data to identify areas favorable for groundwater drilling.

In the sedimentary context, this method can determine the lateral and vertical extent of the basins filling in sedimentary deposits. Additionally, this method facilitates the estimation of water storage capacity within such basins. In the crystalline environment, however, the employment of gravity is primarily focused on the mapping of faults, fractures, and associated weathering effects. These phenomena serve to increase the porosity of rocks and, as a result, enhance their capacity to retain groundwater [9,22,24].

2. Study Area

2.1. Geographical and Climatic Context

The Ifni inlier, with a surface area of 10.360 km^2, is located in the southwestern region of Morocco (Figure 1). It extends between 29°05′ N to 29°45′ N latitude and 9°50′ W to 10°30′ W longitude with a mountainous topography where altitudes vary from 6 to 1236 m. The slopes range from 0 degrees in Wadi beds to 70 degrees in sloping topography areas [37,38]. The northern and southern boundaries of the region are delimited by the Adoudou and Assaka Wadis, respectively, while the eastern border is demarcated by the Lakhssas plateau. The Atlantic Ocean marks the western limit. The hydrological network is well-developed and comprises two main rivers that originate in the inlier relief, namely the Oundera Wadi in the south and Krayma in the north. The climate is semi-arid with highly variable annual rainfall, which averages 133 mm per year [37,38]. The rain is irregular and poorly distributed throughout the year. The average temperature can reach up to 30 °C, with significant monthly and daily variations.

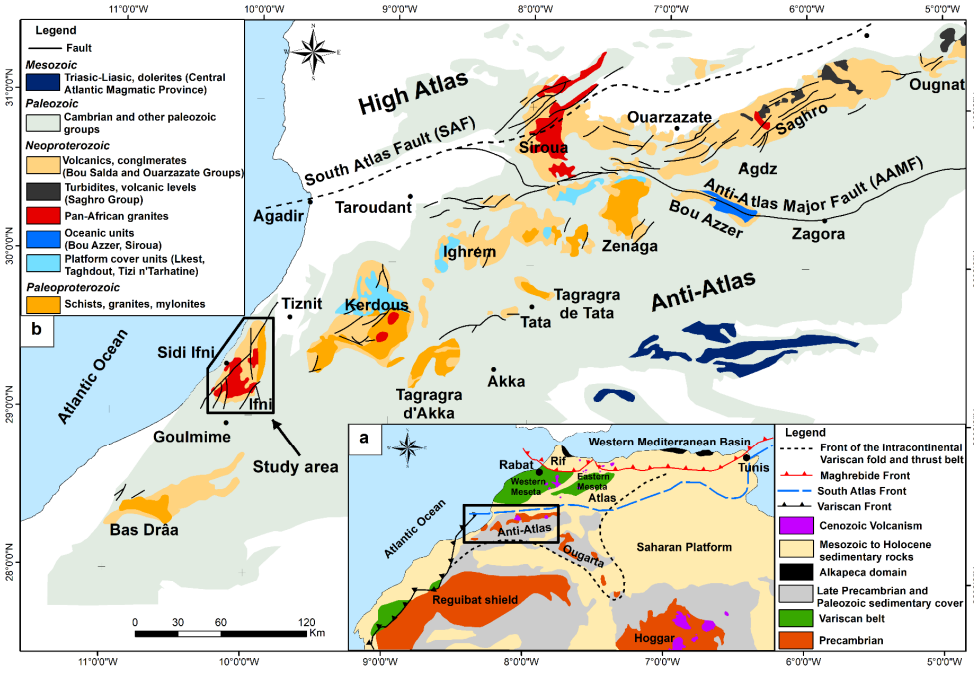

Figure 1. (**a**) Location of the Anti-Atlas in Morocco; (**b**) Location of the study area on a simplified geological map of the Anti-Atlas showing the main Precambrian inliers (Simplified by Hollard et al. [39]; Soulaimani et al. [40]).

2.2. Geological Settings

The Ifni inlier belongs to the Precambrian basement of the western Anti-Atlas Mountain range (Figure 1b). It consists of a crystalline basement formed by a Paleoproterozoic substratum represented by the Alouzad granite, which outcrops to the east of the massif and a lower Neoproterozoic cover represented by the series of quartzitic sandstones and conglomerates of the Lkest group and the volcanic-sedimentary formations belonging to the Ouarzazate group (Figure 2a,b) [41–45]. Late Neoproterozoic granitoid complexes, such as the Sahel massif granodiorites, the Tirhirt granite, the Mesti granodioritic and monzogranitic massif, the Ifni granodioritic massif, the Tioughza granodiorite, the Taoulecht syenogranitic, and the Mirleft granite [5–7], are overlain on these formations. In addition, the Lower Cambrian series, including conglomerates, lower limestones, Lie-de-vin, and Upper Limestones [46–49], are overlain on the Proterozoic assemblages. Additionally, rare Cretaceous deposits have been observed, as well as Quaternary deposits near the Atlantic coast and along the Wadis [41]. From a structural perspective, the Ifni inlier has experienced multiple tectonic events that have impacted the Anti-Atlas chain, including fractures, faults, and schistosity. Brittle tectonics dominates, with fold tectonics and associated foliation being less developed [40,46,47]. The geological map of Ifni at 1:100,000 reveals visible primary directions of N-S and NNE-SSW to ENE-WSE faults that formed during the Eburnian and Panafricain deformation. These fractures intersect with NW-SE structures that can be traced for several kilometers (as depicted in Figure 2a) [41,44,46].

2.3. Hydrogeological Setting

The synthesis of geological, hydrological, and topographical data as well as drilling data obtained from the Drâa-Oued Noun Water Basin Agency, has led to the conclusion that the nature of aquifers in the region is fractured type [5–7]. The location of most of the positive drillings coincides with the passage of faults or fractures [45–47]. Recent work of Ikirri et al. [50] has shown that areas of very high groundwater potential are mainly found in the southern, eastern, and north-eastern plains of the Ifni Basin, particularly at the intersection of the hydrographic network with the hydrogeological lineaments. These areas generally lie in granitic formations, volcanic sedimentary formations, and alluvial plains,

with high porosity and permeability in the low-lying topographic areas. The Tangarfa spring, with a flow rate of 16 L/s, is a good example because it emerges in the contact zone between volcanic rocks and carbonates, facilitated by a network of NE-SE and NW-SE oriented faults [5,7,50]. The high potential areas mainly surround the tributaries of the main river as well as the faults. The Larba-Msti well and the Mesti spring, with high flow rates of 8.33 L/s and 5.66 L/s, respectively, illustrate the synergistic effects of multiple factors favorable to groundwater infiltration. Their presence in highly permeable alluvial deposits, situated above a well-developed drainage network that interconnects with fault systems, highlights the complex interaction of lithologic, hydrologic, and structural controls on groundwater flow dynamics. In the vicinity of the city of Sidi Ifni, granitic and granodioritic formations were studied through 15 boreholes, revealing a positive correlation between water occurrence and fractured levels recorded at variable altitudes [8]. Measured flow rates showed a wide range of variability and in some cases reached significant levels (up to 3 L/s) [44].

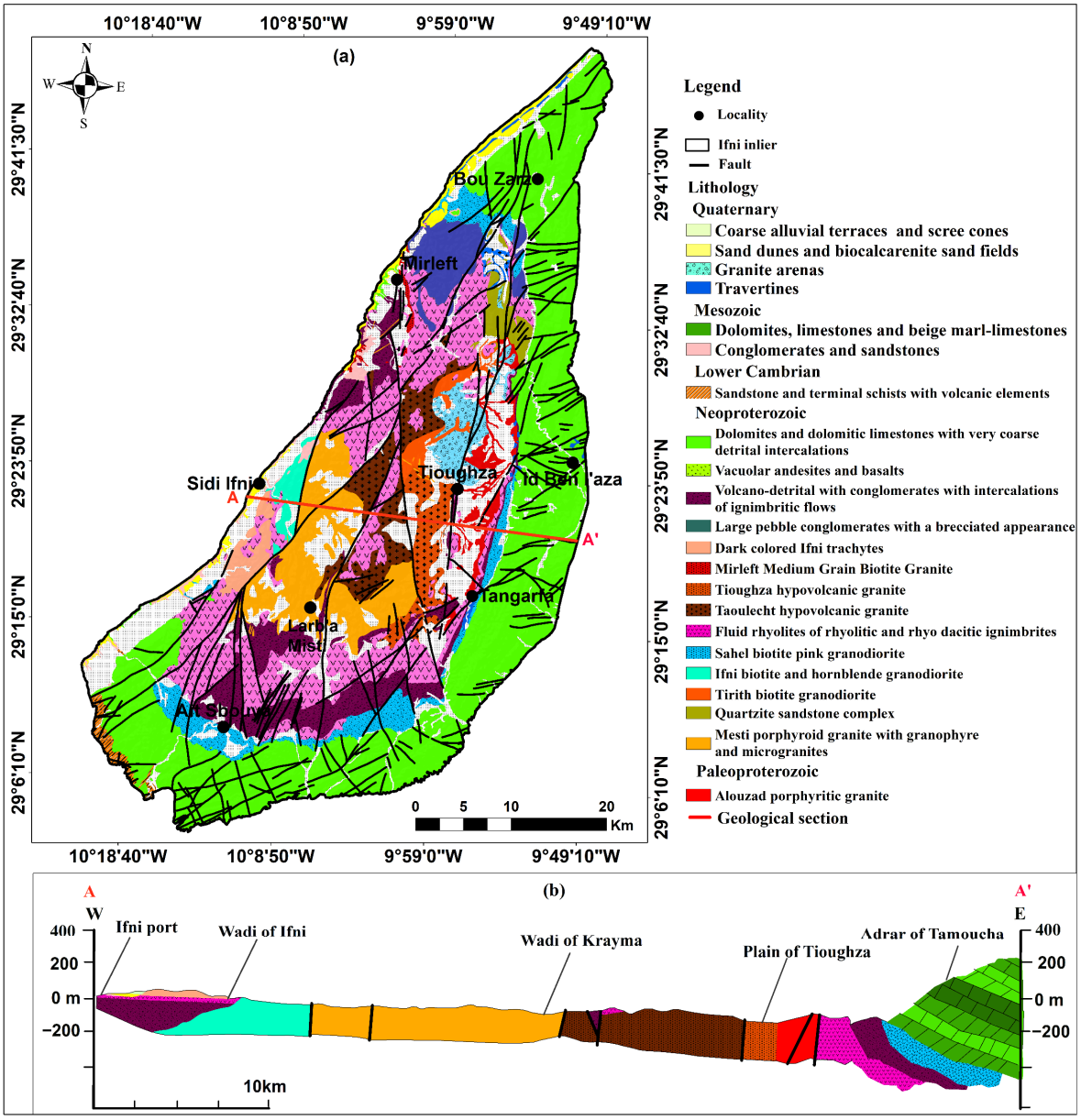

Figure 2. (**a**) Geological map of the Ifni inlier (Extracted from a 1:100,000 map of Sidi Ifni); (**b**) Geological section AA′ across the Ifni inlier.

3. Materials and Methods

3.1. Gravity Prospection

This research uses a methodology that interprets gravity data from a national mapping project initiated by the Geology Directorate of the Moroccan Ministry of Energy and Mines in the late 1970s. The data is available as a Bouguer anomaly map, calculated using a correction density of 2.67 g/cm^3 [51,52]. The gravity data were collected at intervals of 1 to 5 km along roads and pathways, with a higher concentration in plains than in mountainous areas. To process and analyze this data, the Bouguer anomaly map was initially digitized from a scanned image and then interpolated at the nodes of a uniform mesh. This allowed for representation as a color image (as shown in Figure 3) and transformation and filtering necessary for interpretation [9,13,26,28,31,53–58].

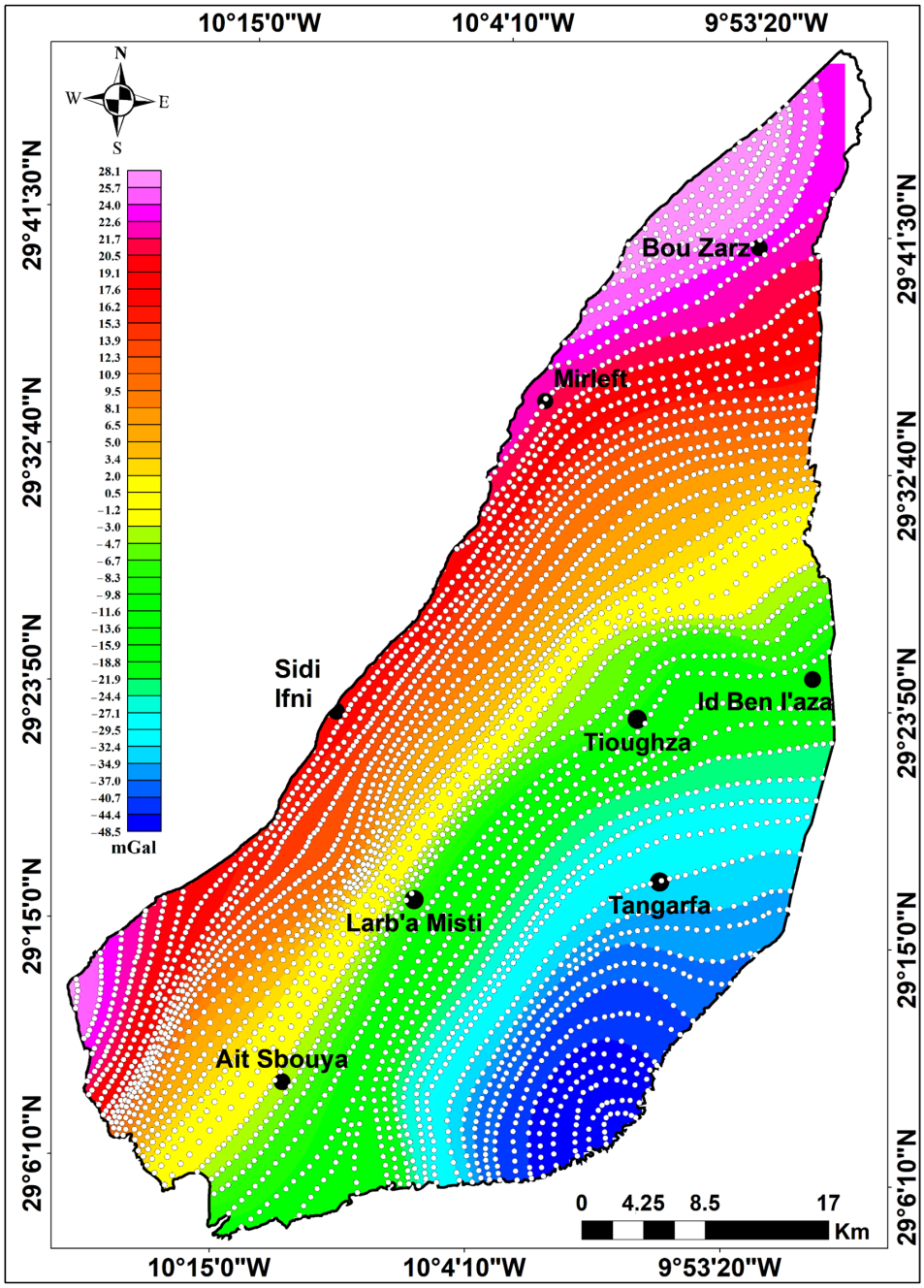

Figure 3. Bouguer anomaly map of the Ifni inlier obtained by interpolating digitized gravity data; White dots represent gravity data sampling during the digitization process.

To obtain comprehensive information about the spatial arrangement of tectonic structures relevant to hydrogeology in the study area, we used Geosoft mapping and processing software to subject the gravity data to a series of mathematical treatments. First, we removed the regional anomaly and used the total horizontal gradient and Tilt derivative filters as powerful techniques for mapping subsurface geological structures [19,20,26,28,58–64]. Next, we applied Euler Deconvolution to determine the depth location of faults and trace their connection with basement structures [26,54]. Finally, we followed the processing sequence depicted in Figure 4a to analyze and interpret the gravity data.

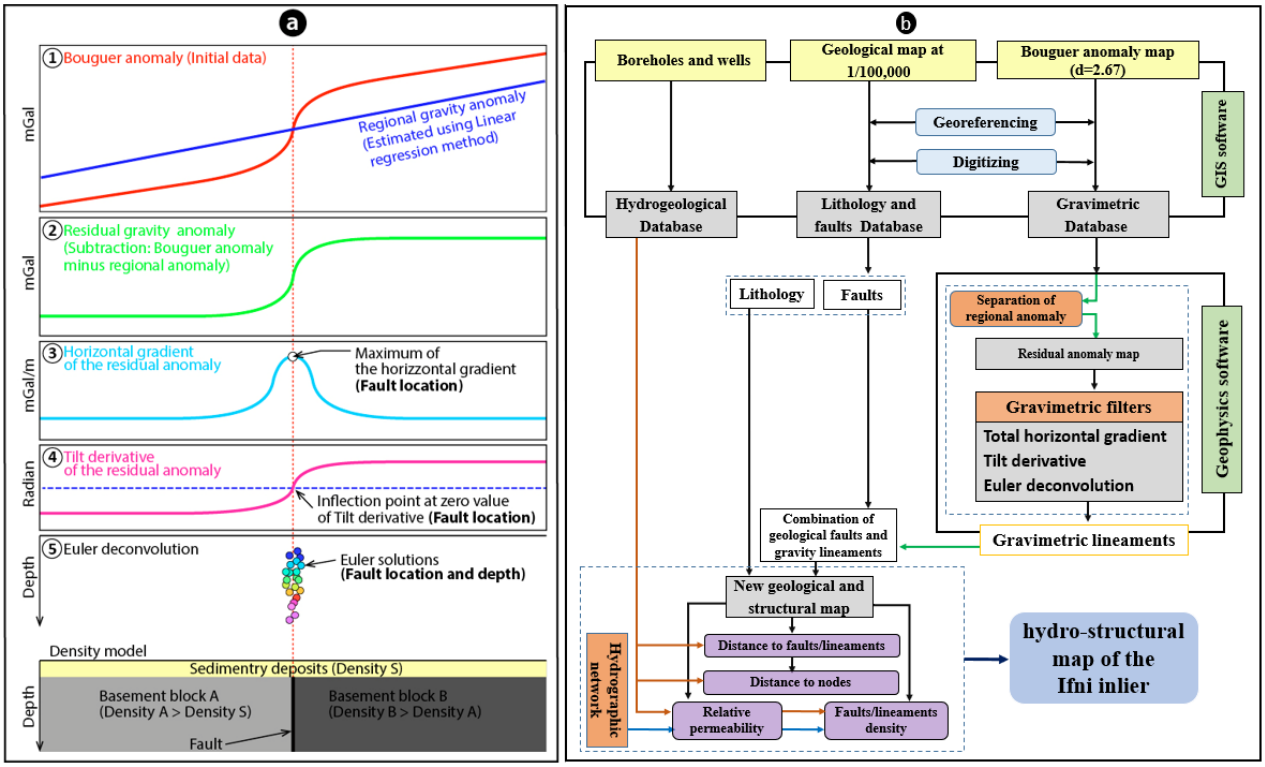

Figure 4. (**a**) Processing sequence applied to the gravimetric data of the Ifni Inlier; (**b**) Illustration of the methodological approach used in the present study.

3.1.1. The Total Horizontal Gradient

The Total Horizontal Gradient (THG) technique is commonly used to locate subsurface discontinuities. It is particularly effective in identifying gradient zones associated with geological contacts or faults [26,35,58,59,61]. These gradient zones indicate boundaries between blocks of varying densities, and maxima typically indicate them (Figure 4a). For this study, we applied the THG technique to the residual anomaly map, using Equation (1) [18,23,27,28,36,65].

$$\mathrm{THG}\ (\mathrm{X},\ \mathrm{Y}) = \sqrt{\left(\frac{\delta g(\mathrm{X},\mathrm{Y})}{\delta \mathrm{X}}\right)^2 + \left(\frac{\delta g(\mathrm{X},\mathrm{Y})}{\delta \mathrm{Y}}\right)^2} \quad (1)$$

where g(X, Y) is the value of the residual anomaly at point (X, Y).

3.1.2. Tilt Derivative or Tilt Angle

The Tilt Angle Transformation is a widely-used method for identifying the edges of sources regardless of their amplitude or depth. This technique is beneficial for analyzing anomalies' texture, appearance, and orientation. The tilt angle is measured in radians, and its zero value corresponds to the vertical boundary of the structure ($\theta = 0$) (Figure 4a). Therefore, the edges of dominant gravitational sources coincide with the tilt angle's zero

value. The transformation process entails calculating the inverse of the tangent of the ratio between the vertical derivative and the total horizontal derivative of the residual anomaly, as demonstrated in Equation (2).

$$\theta = \tan^{-1} \frac{\frac{\vartheta g(X,Y)}{\vartheta Z}}{\sqrt{\left(\frac{\vartheta g(X,Y)}{\vartheta x}\right)^2 + \left(\frac{\vartheta g(X,Y)}{\vartheta y}\right)^2}} \quad (2)$$

where θ and g(X, Y) are the tilt angle and residual anomaly, respectively.

The Tilt derivative has the advantage of reducing the gaps between anomalies and, therefore, better enhances low amplitude anomalies [26,66].

3.1.3. Location of Maxima

The method of approximating the edges of gravity anomalies' sources was employed in this study to locate the THG maxima [62]. This technique is typically used to determine the position of gravity anomalies' sources that correspond to two-dimensional structures, such as faults and linear contacts that separate blocks of varying densities. These structures are particularly interesting in this study as they can help highlight the boundaries between different density blocks [9,19].

The location of THG maxima involves comparing the value at each grid node to its eight nearest neighbors (Figure 5). To find whether the $g_{i,j}$ is the maximum horizontal gradient or not, its eight nearest neighbors must be known and the following conditions should be satisfied [61]:

$$g_{i-1,j} < g_{i,j} > g_{i+1,j}$$
$$g_{i,j-1} < g_{i,j} > g_{i,j+1}$$
$$g_{i-1,j-1} < g_{i,j} > g_{i+1,j+1}$$
$$g_{i+1,j-1} < g_{i,j} > g_{i-1,j+1}$$

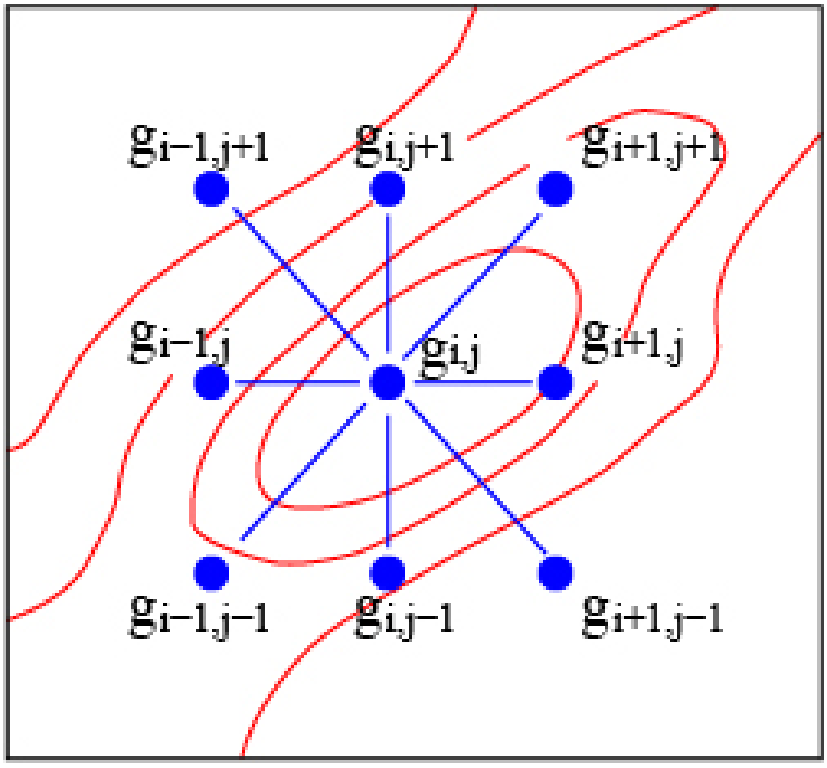

Figure 5. Location of grid nodes used to search for a maximum around $g_{i,j}$. Red curved lines represent contours of horizontal gradient values of gravity anomalies [61].

3.1.4. Euler Deconvolution

The Euler deconvolution technique, initially proposed by Thompson [66], is a filtering method that facilitates the characterization of geological structures by enabling the detection of their location, determining their depth, and identifying their degree of rooting (Figure 4a) [17,18,67]. Numerous research studies have extensively validated this technique [11,13,29,30,68–70]. The "structural index" parameter is a crucial factor for selecting the type of structures to be emphasized, with integer values ranging from 0 to 3. The other essential parameter is the size of the moving window, which depends on the wavelength of the anomalies under investigation [34,71]. Using a small window may not allow for proper interpretation of long wavelength anomalies, whereas selecting a large window can introduce the effects of multiple sources, leading to a cloud of ill-defined solutions that obscure the best solutions [15,26,70,72]. For example, given a source S located at point M with coordinates (X_0, Y_0, Z_0), the gravimetric field intensity F at the observation point can be computed using Equation (3) [15,26,29,30,33].

$$F(X, Y) = f[(X - X_0), (Y - Y_0), (Z - Z_0)] \quad (3)$$

Thompson [66] showed that the Euler homogeneity equation can be written as (Equation (4)):

$$(X - X_0)\frac{\vartheta F}{\vartheta x} + (Y - Y_0)\frac{\vartheta F}{\vartheta y} + (Z - Z_0)\frac{\vartheta F}{\vartheta z} = -NT(B - F) \quad (4)$$

(X_0, Y_0, Z_0): Position of the gravimetric anomaly source,
(X, Y, Z): Position of the observation point,
F: Intensity of the gravity field measured at the point (X, Y, Z),
B: Regional value of the gravity field,
N: Degree of homogeneity or structural index (SI) that characterizes the type of source and rate of change of the field as a function of distance.

The principle of the method is based on solving a system of equations with four unknowns: X_0, Y_0, Z_0, and B.

The present study used the Euler deconvolution technique with a structural index of IS = 0, a moving window size equivalent to nine times the dimension of the unit cell of the interpolation grid, and a tolerance level of 15%. After applying mathematical treatment to the gravity data, a field of lineaments with varying lengths and extensions was identified. These lineaments were then superimposed on a geological map that included structures and lithology, producing a new structural map for the study area. Additionally, data on flow rates and permeability acquired from hydrogeological reconnaissance boreholes and wells were integrated into the map. As a result, a hydro-structural map of the Ifni inlier was developed. A summary of the methodological approach utilized in this study is presented in Figure 4b.

3.2. Geological Data

The determination of favorable areas for groundwater exploitation in crystalline basement terrains depends largely on geological factors [73–76]. Faulting and high permeability are key elements that allow water to infiltrate, increasing permeability and secondary porosity, and favoring vertical water flow to recharge the aquifer [50,76–79].

In this study, the lineament map initially generated by gravimetric processing was combined with the geological fault map digitized from the Ifni geological map. The lineament density was calculated using the linear density function in the ArcGIS spatial analysis extension. It is important to note that hydrogeological exploration must take into account the proximity of networks and fracture nodes, as outlined in several recent studies. Hydrogeological exploration requires careful consideration of distances to fault networks and fracture nodes, as outlined in several recent studies (e.g., [76,77]).

In the Ifni inlier, the relationship between boreholes and fractures can be very instructive in understanding the hydraulic effects of tectonic faults in different directions (N-S,

NNE-SSW, NE-SW, ENE-WSW, NW-SE, and E-W). We measured the distances between each positive well and borehole and the fractures in each of the six main directions and their intersections by overlaying the database of positive water points (199 points) on the lineament map. This step lets us test the influence of fracturing on drilling performance. The permeability of the area is closely related to tectonic structures, such as faults and flexures [5–8]. The relative permeability of the Ifni inlier was generated from the 1:100,000 scale geological map using the method of transforming the values of this parameter into a logistic space. This method provides additional discriminating information to aid in interpreting permeability data [76,80–84]. The database of positive water points was overlaid on the permeability map to test the impact of this factor on borehole performance.

3.3. Resistivity Data

Resistivity data plays an important role in identifying and mapping potential groundwater areas [85,86]. Apparent resistivity is a measure of the ability of a material to withstand the passage of an electric current. Areas of low resistivity may indicate the presence of saturated groundwater, while areas of high resistivity may correspond to more resistant rock or soil [86,87]. In this study, the apparent resistivity map at a frequency of 7200 Hz at a scale of 1:100,000 was used to determine the negative and positive anomalies of the Larb a Misti geological formations. The apparent resistivity anomaly values were compared with those represented on the gravity anomaly maps. It was also used to assess the productivity of the drill holes drilled. This map was provided by the Geology Directorate of the Moroccan Ministry of Energy and Mines in late 2001. In general, low frequencies penetrate deeper, but provide a less detailed resolution of shallow features. In this study, the depth of investigation is determined using Equation (5) and based on the average resistivity of the geological formations in the area [88–92].

$$\delta = 503 \sqrt{\frac{\rho}{f}} \quad (5)$$

where 503, ρ and f are constant, the average resistivity (Ohm.m) and Frequency (Hz), respectively.

4. Results and Discussion

4.1. Gravimetric Analysis

Upon examining the Bouguer anomaly map, the first notable observation is a regional gradient characterized by a gradual increase in values from the southeast to the northwest (Figure 3). This trend is likely a result of crustal thinning from the continent to the ocean. These large-scale variations of deep origin, which range from −48.5 mGal to 28.1 mGal, obscure specific gravity signatures, particularly those of low amplitude, such as gradient zones. To better discern these signatures, it is necessary to remove the regional component. The regional component was estimated by a plane calculated using the first-order polynomial regression method [26,33,58,58,59,93]. By subtracting this component from the initial data, the residual anomaly map shown in Figure 5 was obtained [20,58,59,94,95]. A detailed analysis of the resulting residual map reveals several positive (PA1 to PA4) and negative (NA1 and NA2) anomalies with values ranging from −16.6 mGal to 8.2 mGal (as seen in Figure 6). These anomalies reflect lateral variations in subsurface density over the study area, which are generated by geological structures of varying sizes, depths, and directions. They are defined as an average background level that is primarily represented by the green and yellow shades characterizing the Neoproterozoic formations of the Ifni inlier (depicted in Figure 2).

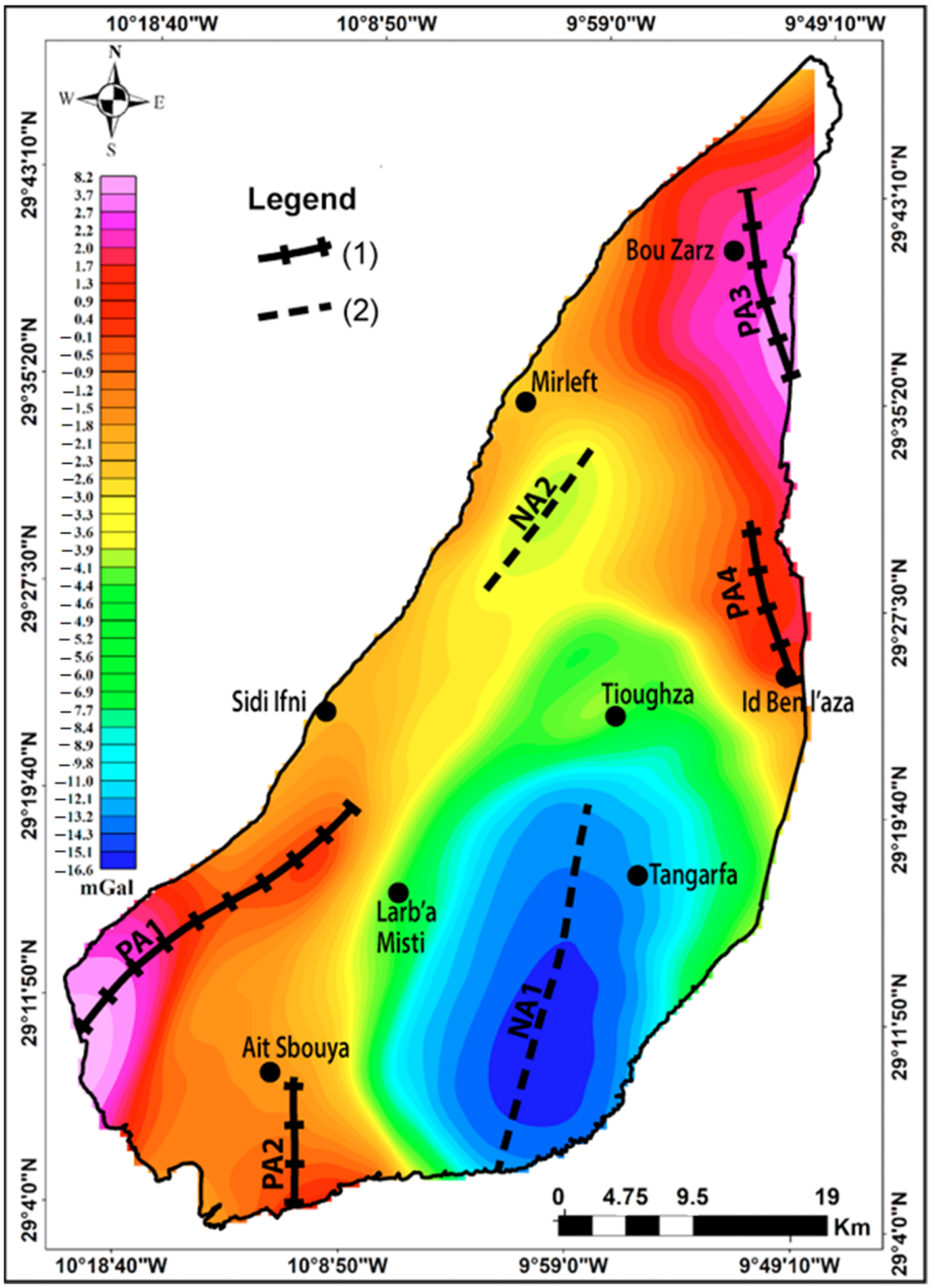

Figure 6. Residual gravity anomaly map of the Ifni inlier: (1) Axis of a positive anomaly; (2) Axis of negative anomaly.

The map (Figure 6) is notably dominated by the negative anomaly (NA1), which coincides with relatively low-density crystalline fractured and volcano-sedimentary terrains situated south of the study area. A second negative anomaly is observed to the south of the Mirleft locality, elongated in a NE-SW direction and coinciding with alluvial formations and older sedimentary terrains that could constitute graben fillings and highly fractured crystal formations. The positive anomalies represented by the orange, red, and purple shades occupy the northeastern and southwestern parts of the study area. They are generally superimposed with formations of the Paleozoic cover, primarily composed of Lower and Middle Cambrian carbonate. Raised features of the crystalline basement can explain them

under this cover or by horsts structures. The anomaly (PA1) is situated at the extreme southwest of the study area and is represented by an increase in residual gravity values that reaches a maximum of 8.2 mGal. This anomaly corresponds to the southwestern end of a positive axis that extends further northeast, where its amplitude significantly decreases. It could correspond to a rise in the basement. The positive anomalies PA2, PA3, and PA4, generally NW-SE, coincide with areas of dolomite and limestone cover. They can also be explained by the local rises of the Precambrian basement under the cover.

Various filtering procedures were implemented on the residual anomaly map to obtain a comprehensive mapping of geological structures associated with gravity gradient zones. The presence of faults or contacts that separate blocks with different densities and abrupt lithological changes can be indicated by gravity gradients found at transition zones between positive and negative anomalies. To identify areas of interest for hydrogeological investigations of the Ifni inlier, the Total Horizontal Gradient (THG) of the residual anomaly map was calculated, and the maxima were located (as shown in Figure 7a). The structures identified using this filtering technique, including major faults (designated as F1 to F11) and minor faults represented by continuous and dashed lines, varied in length. The results showed that NE-SW trending structures were predominant, intersecting by E-W and NW-SE trending structures in some locations. While some major faults, such as F1, F9, F11, and half of F10, intersected the Paleozoic cover, others mainly affected the Precambrian basement of the Ifni inlier over a few tens of kilometers. Faults F1 to F8 were typically oriented NE-SW, parallel to the Atlantic margin, whereas the other three faults (F9, F10, and F11) were generally perpendicular to this margin. Overlaying all the structures on the residual gravity map determined their positions based on the positive and negative anomalies (as depicted in Figure 7b). This highlighted the crucial role of these structures, particularly the major faults, in shaping the Precambrian bedrock of the Ifni inlier. These faults are likely responsible for the undulations of the bedrock topography beneath the Paleozoic cover, which could account for the observed anomalies.

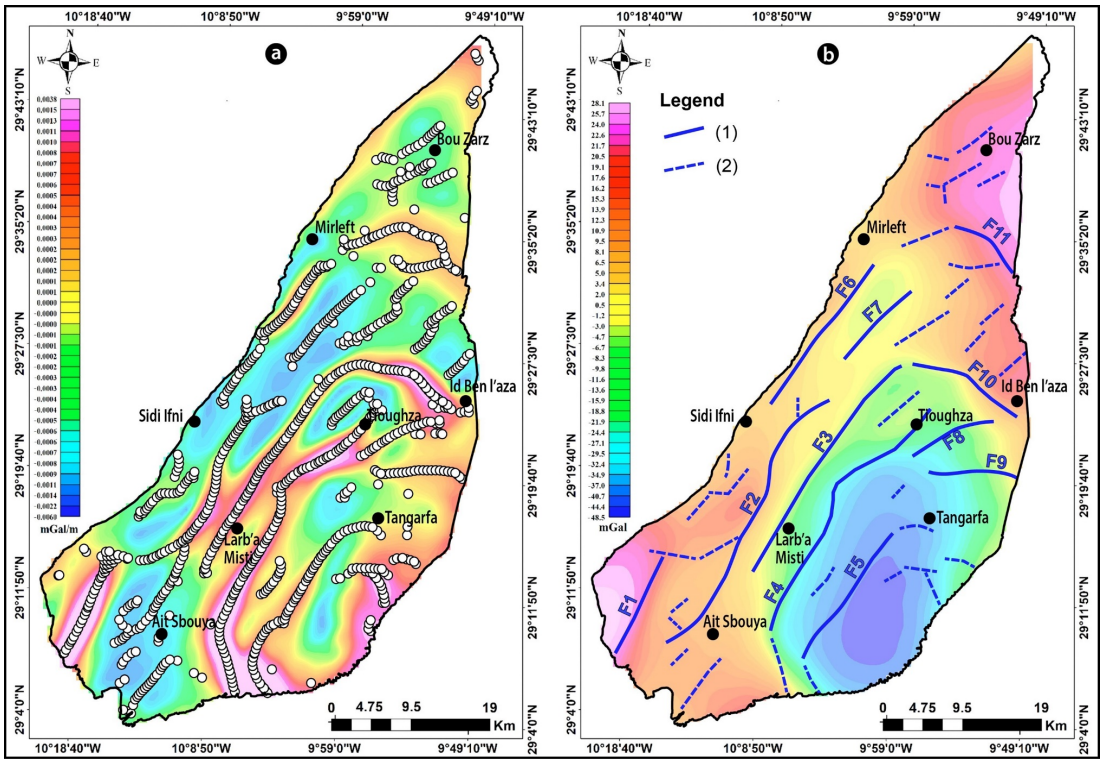

Figure 7. (**a**) Maxima of the THG map of the Ifni inlier; (**b**) Superimposition of the interpreted structures from the THG maxima to the residual anomaly map: (1) Interpreted major gravity fault; (2) Interpreted minor gravity fault.

In addition, we applied the Tilt angle filter to the residual anomaly map as a secondary method for detecting gravity contacts. Zero contours typically indicate these contacts, represented by the white dashed line. This contour coincided with most of the faults identified by the THG technique, supporting their presence as structural characteristics of the study area (see Figure 8a). Moreover, we utilized the Euler deconvolution technique on the gravity data to further characterize the geological structures based on their rooting depth. We computed solutions corresponding to fault-like structures with a structural index (SI) of zero, a maximum relative error (T) of 15%, and a moving window size (W) of 10 × 10. These solutions are presented in Figure 8b, together with the faults identified by the THG method. Upon examining this figure, we observed that the most closely clustered solutions are located along the detected faults. Thus, the Euler deconvolution not only confirmed the existence of the faults identified by the THG method but also provided additional information regarding their depth.

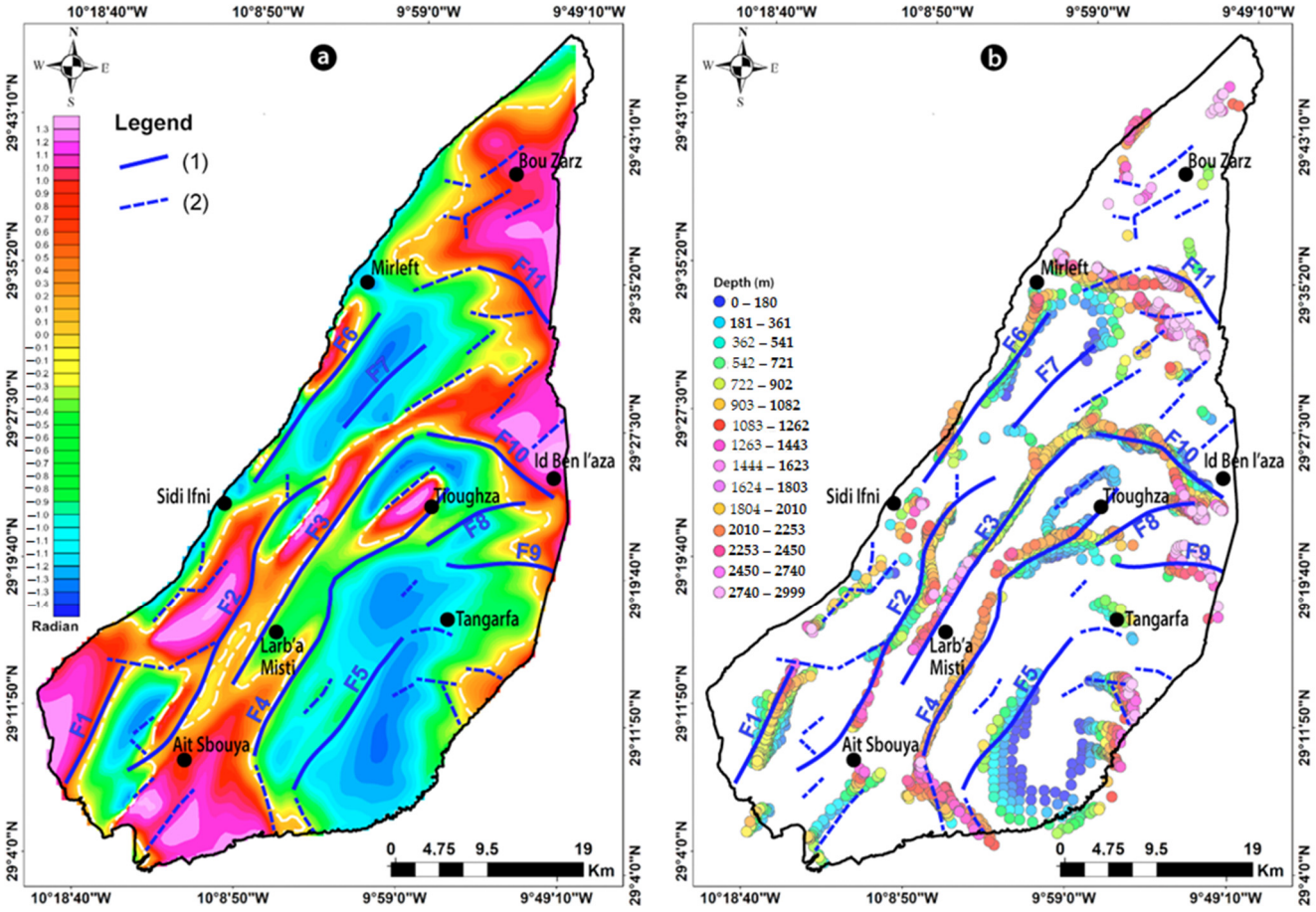

Figure 8. (**a**) Structures interpreted from the THG map of the Ifni inlier overlaid to the Tilt derivative map: (1) Interpreted major gravity fault; (2) Interpreted minor gravity fault; (**b**) Superimposition of the same structures to the Euler solutions was calculated using a structural index SI = 0, a moving window of 10 × 10, and a maximum relative error of 15%.

The new faults, inferred from the gravity data, were superimposed on the Ifni inlier's structural map (refer to Figure 9), resulting in an updated map. After a more thorough analysis of this updated map, it was found that some of the interpreted structures had not been included in the original geological map. However, some of the new structures corroborated the existence of previously observed faults, partially or entirely coinciding with them. These findings indicate that the current study has contributed to a more thorough characterization of the deep structure of the Ifni inlier by providing valuable insights into the fault system that impacts this Precambrian section of the Anti-Atlas range.

Additionally, the newly identified faults may represent concealed structures buried beneath recent sedimentary deposits and harboring high-potential groundwater that may have remained undetected by surface geological observations. The rose diagrams established separately for the observed faults and those inferred from gravity data show that the study area is affected by a network of faults of different orientations. The observed faults are organized along a range of directions varying from NNW-SSE to E-W with a predominance of N-S and ENE-WSW orientations (Figure 9b). However, the direction of the faults interpreted from the gravity data is dominated by the NE-SW trend (Figure 9c). This difference in the shape shown by the two rose diagrams is explained by the fact that the observed faults include a large number of minor accidents of low horizontal extension that mainly affect the Paleozoic cover and whose slip does not allow the contact of blocks with a significant density contrast. Such faults cannot be detected by the gravimetry method. The new structural scheme thus developed highlights two main fault families.

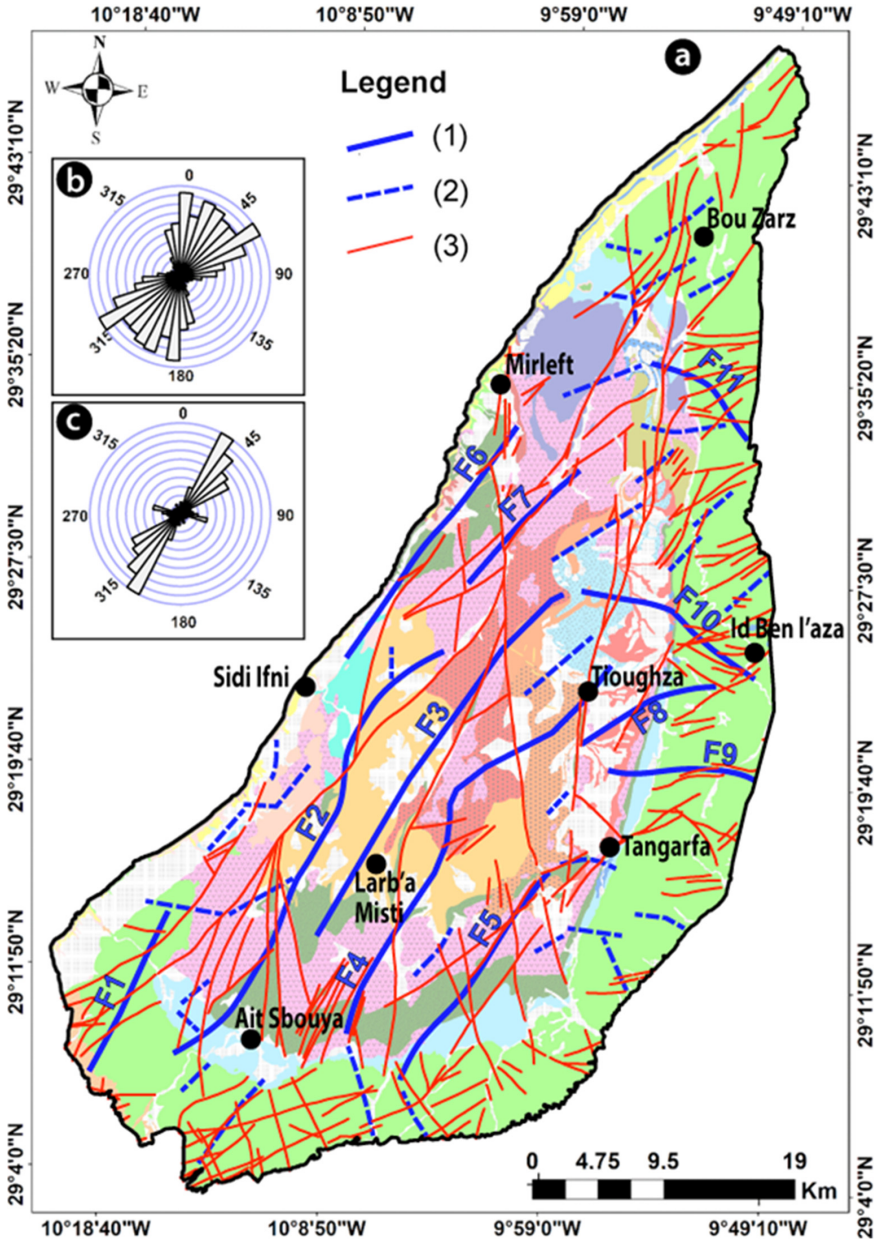

Figure 9. (**a**) Structural map of the inlier Ifni superimposed on the geological map: (1) Interpreted major gravity fault; (2) Interpreted minor gravity fault; (3) Observed geological faults (same legend as Figure 2a); (**b**) Observed geological faults rose diagram; (**c**) Interpreted gravity faults rose diagram.

The first one of the average NE-SW directions is parallel to the major structural direction of the Anti-Atlas chain and the general elongation of the Ifni inlier. The second family, generally perpendicular to the first, with an average NW-SE orientation, corresponds to structures associated with events affecting the area during the Eburnian and Pan-African orogeny [5,41,42,46,48,94].

4.2. Impact of the Structural Context on Hydrogeological Potential

The impact of faults on hydrogeological groundwater potentialities was carried out through a comparison of data from 199 wells executed in the study area. The fault's effect on groundwater availability is most evident in Figure 10a. More than 80% of the positive wells are located in areas with high fracture density values. The highest flow rates of these wells are found in the Tioughza and Larba-Mesti areas, characterized by the combination of high lineament density and good permeability of the formations (Figure 10a,b). The lithological map of the Ifni inlier comprises formations composed of the Quaternary complex of high permeability comprising mainly alluvial deposits representing 18.72% of the surface. The area is dominated by crystalline formations (granitoid and granite), volcano-detrital with conglomerates, dolomitic limestones, and quartzite sandstones presenting a permeability of fractures, occupying 81.28% of the area (Figure 10b).

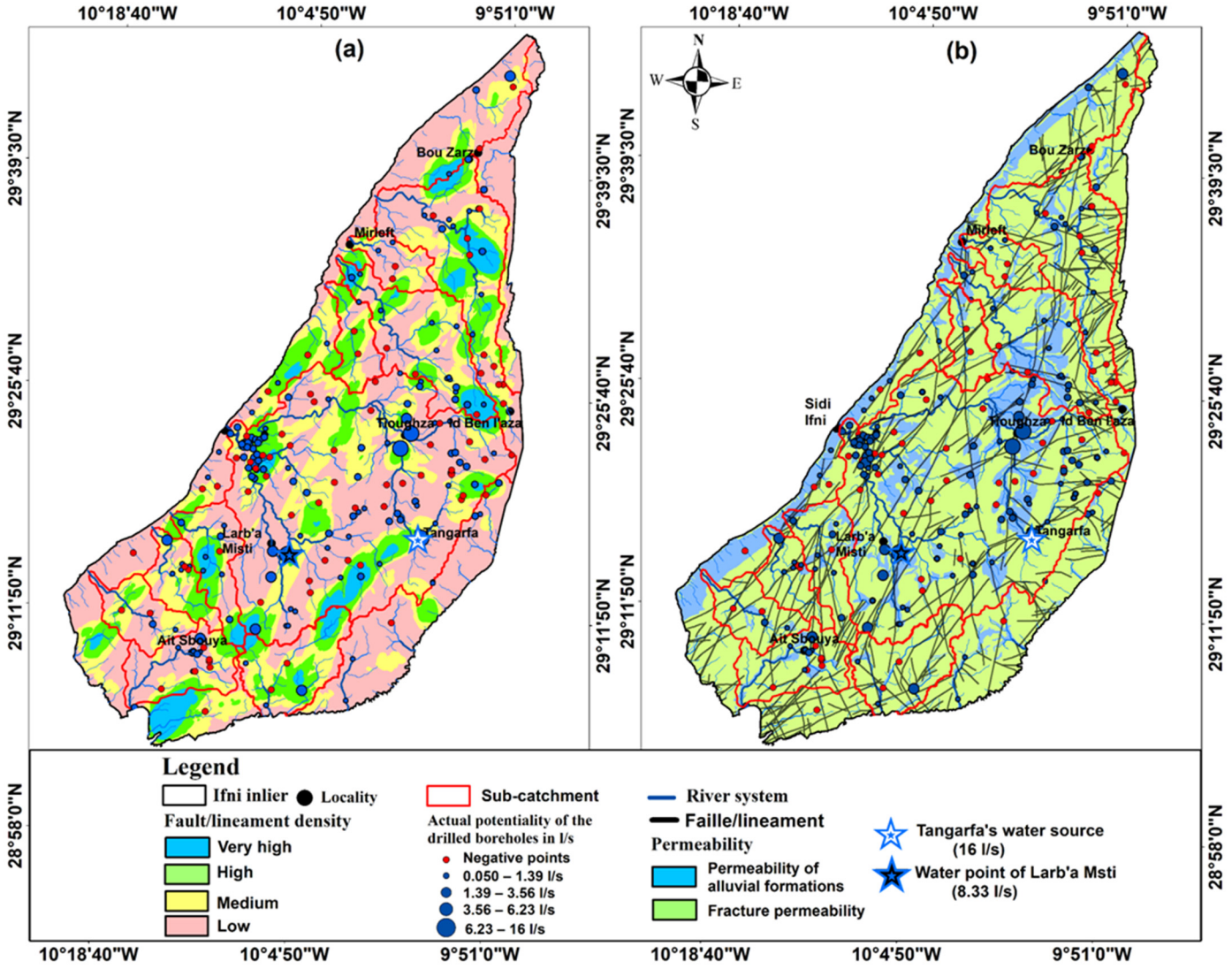

Figure 10. Superposition of the fault network and water points on the faults/lineament density (**a**) and permeability map (**b**) of the Ifni inlier.

Wells with positive yields are generally located along rivers and faults in alluvial, granitic, and volcano-sedimentary formations. Boreholes with very high flow rates are mainly located in the southern, eastern, and northeastern plains, particularly at the intersections of the river system and the main hydrogeological faults affecting the Ifni inlier. Indeed, groundwater accumulation zones are formed where the main hydrogeological faults intersect the hydrographic network. These zones, which have high permeability, generally extend over granitic formations, volcanic sedimentary formations, granitic sands, and alluvial plains, and can be a crucial source of water for wells.

The Tangarfa spring, with a flow rate of 16 L/s, is an excellent example as it emerges in the contact zone between volcanic and carbonates rocks (fracture permeability), facilitated by a network of NE-SE and NW-SE oriented faults (Figure 10b). High flow rates mainly encircle the tributaries of the main river and the faults. The Larba-Msti well and The Mesti Spring, with respectively high discharge rates of 8.33 L/s and 5.66 L/s, exemplify the synergistic effects of multiple favorable factors for groundwater infiltration. Their occurrence in highly permeable alluvial deposits, situated above a well-developed hydrographic network that interconnects with fault systems, highlights the complex interplay of lithological, hydrological, and structural controls on groundwater flow dynamics.

A study conducted by Aude [8] on granitic and granodiorite formations in the vicinity of the city of Sidi Ifni involved 15 boreholes. This study showed a positive correlation between the presence of water and fracture levels at different depths [8]. Specifically, fracture levels have been observed at different depths and have been associated with the presence of groundwater in granitic and granodioritic rock. The measured flow rates revealed a high variability and reached significant levels (up to 3 L/s) in some cases (Figure 11, Table 1), similar to those obtained in other study areas [5–8,87]. However, boreholes drilled on the slopes of bare mountains, ridges, and hills with steep slopes and high runoff revealed low flows. These areas are characterized by low fracture permeability of the igneous formations, poor surface drainage, and low lineament density. This study revealed varied results in terms of water flow rates depending on the geological and topographical characteristics of each area.

Table 1. Hydro-structural characteristics of the 15 boreholes drilled in the granitic basement of Ifni [8,87].

Borehole	X	Y	Total Depth	Lithological Formation	% of the Cumul Length Fractured Formation	Yield of Borehole (L/s)	Permeability
S1	40,767	274,334	80	Gd	12%	0.05	-
S2	41,381	274,956	32	Gr	60%	3.5	5.32×10^{-8}
S3	41,192	273,889	32	Gr	66%	0.5	1.18×10^{-7}
S4	41,107	273,605	42	Gr	36%	1.8	1.04×10^{-6}
S5	40,292	270,074	80	Gd	26%	0.08	-
S6	40,209	270,323	60	Gd	16%	0.02	1.27×10^{-6}
S7	39,667	271,138	50	Gd	20%	-	-
S8	41,829	271,506	80	G	32%	0.55	1.07×10^{-7}
S9	40,528	271,663	50	Gd	14%	0.6	4.3×10^{-7}
S10	40,998	271,739	80	Gd	25%	0.45	0.95×10^{-7}
S11	41,356	270,658	80	G	55%	1.4	-
S12	40,710	271,121	50	G	14%	0.06	-
S13	40,643	273,948	80	Gd	25%	0.3	0.9×10^{-7}
S14	39,380	273,811	60	Gd	12%	0.02	-
S15	39,784	273,385	80	Gd	0%	-	-

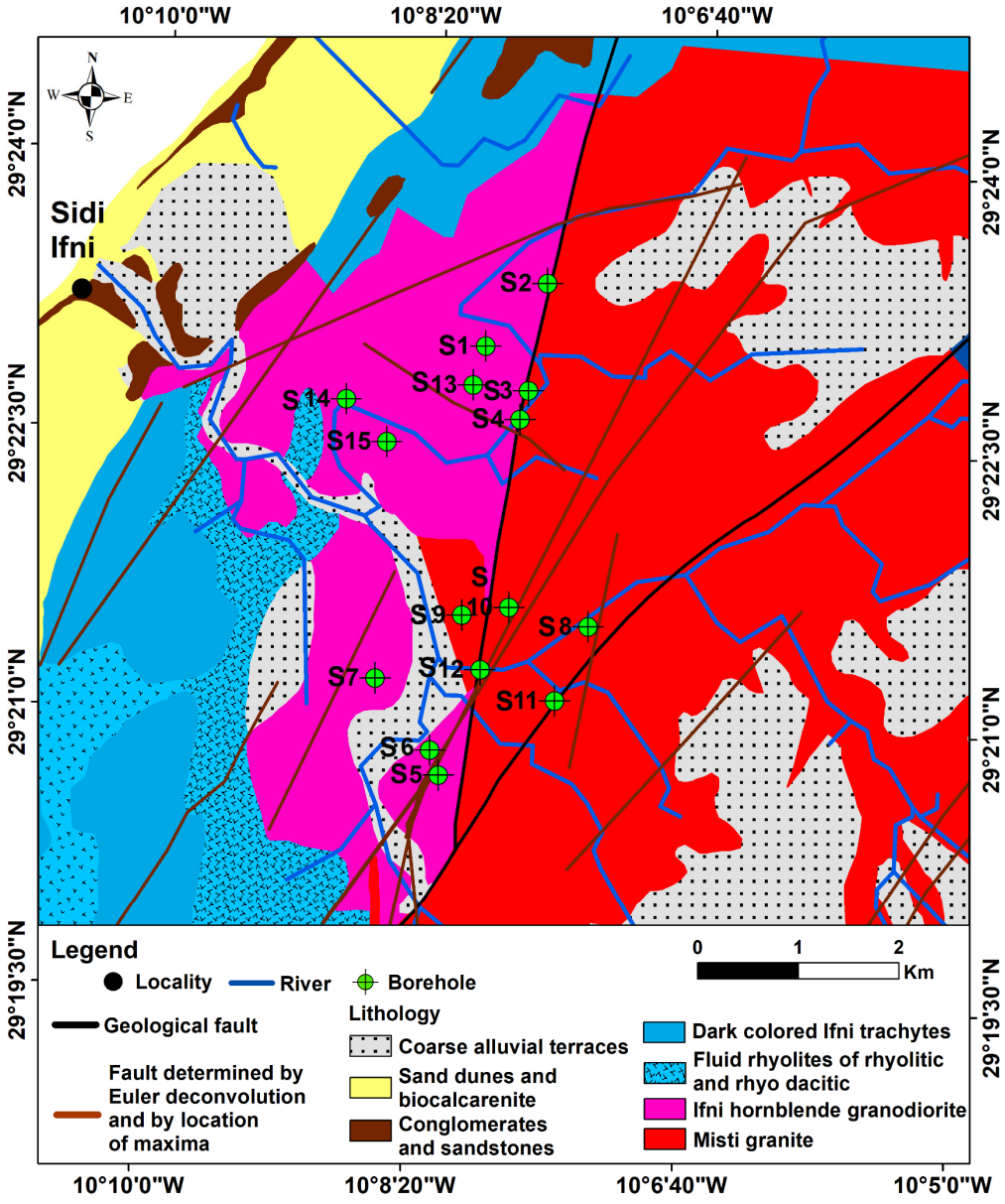

Figure 11. Location of reconnaissance boreholes (S1 to S15).

The newly created structural map (Figure 9), was used to measure the distances between the positive water wells and the tectonic faults. The analysis revealed that 35.24% of these wells are located within 100 m, while 21.23% are located between 100 and 200 m. Furthermore, 26.85% of the wells are located between 200 and 400 m, and only 16.68% are located beyond 400 m (Figure 12). These results demonstrate a strong and significant correlation between the presence of positive water points and the proximity of faults and tectonic nodes. Therefore, it is evident that these structures have a significant impact on groundwater flow and aquifer recharge in the study area.

To confirm the impact of faults on groundwater potential in the study area, the high-resolution (7200 Hz) electrical resistivity map, although covering a small area (Larb a Misti) compared to the gravity data, was used (Figure 13). The relatively high frequency of 7200 Hz was used for shallow subsurface imaging with a penetration depth of 84 to 187 m (Table 2). The negative boreholes (S16 to 21) are located in high resistivity ranges (1024 Ohm.m) corresponding to sound basement formations without fault crossings. On the other hand, the positive boreholes (S1 to S15) are located in anomalies of low linear resistivity reflecting the impact of fault crossings, which, thanks to the water they drain, tend to decrease the

resistivity values of the formations. Resistivity data can provide valuable information for mapping and identifying potential groundwater zones by helping to identify subsurface areas and geological features that may influence the movement and availability of groundwater.

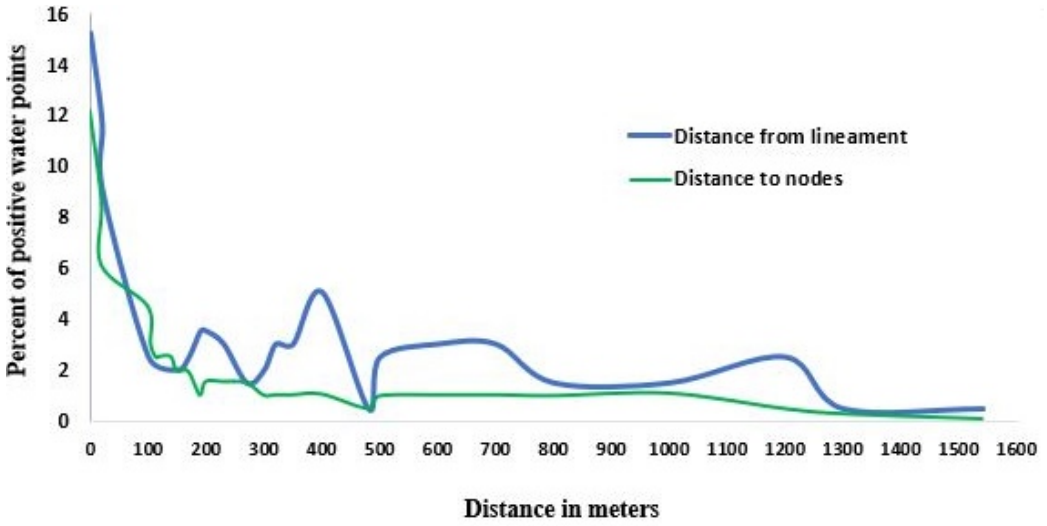

Figure 12. Section of decrease in percentages of positive water points as a function of distance to fractures and nodes in the Ifni inlier.

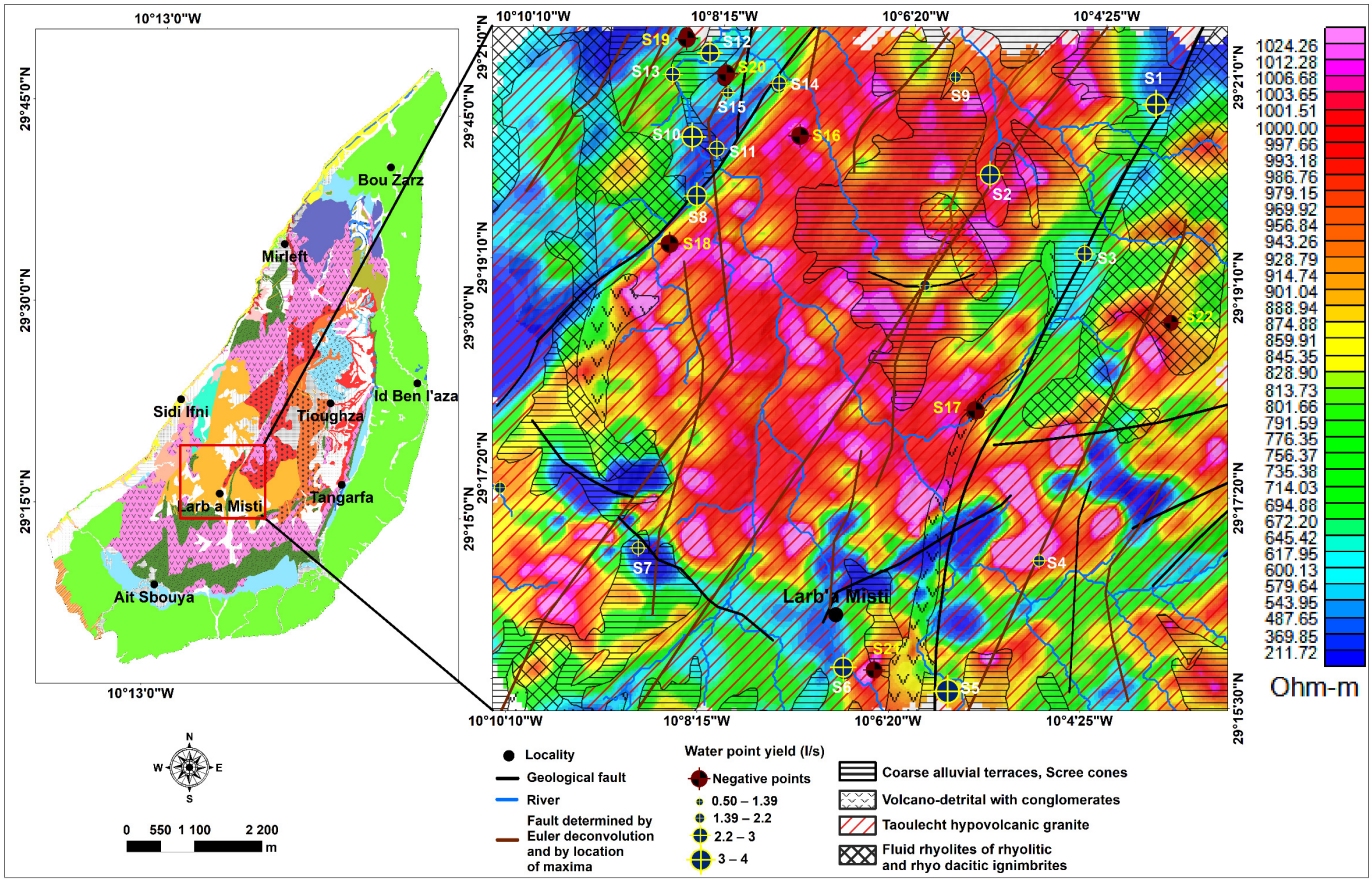

Figure 13. Spatial distribution of apparent resistivity anomalies in the Larb a Misti area superposed by faults and water boreholes (S1 to S15).

Table 2. Depth of investigation of apparent resistivity at frequency 7200 Hz in the Larb a Misti area.

Average Resistivity (Ohm.m)	Frequency (Hz)	Constant	Depth
200	7200	503	84
400	7200	503	119
800	7200	503	168
1000	7200	503	187

5. Conclusions

The structure of the Ifni inlier was better understood through the interpretation of its gravity and electrical resistivity data. These data were obtained by digitizing the scanned maps as we did not have access to the original data. However, being aware that digitization could affect the quality of the data, we ensured that this task was carried out meticulously and with sufficient sample density to faithfully reproduce the original map.

Furthermore, it is worth noting that the hydrogeological implications of this study are limited to fault mapping, including those hidden by recent sedimentary deposits, using the gravity method as a potent tool to detect lateral changes in rock density. The methodology employed in this study utilized classical techniques such as total horizontal gradient and Tilt derivative to detect faults from gravity maps and Euler deconvolution to determine their depth. Additionally, hydrogeologic data, such as relative permeability and groundwater flow, were analyzed to assess the significance of faults on the well's productivity.

The resulting structural map has identified new tectonic features and confirmed the presence of previously known faults. These faults have been characterized in terms of their lateral extension, depth, and importance. The Ifni inlier is seen to be intersected by a network of faults organized into two prominent families that trend NE-SW and NW-SE. Hydrogeological data has been analyzed alongside the structural map to highlight the significance of these faults as conduits for groundwater flow.

Discontinuities such as faults and joints provide opportunities for hydrogeological exploration drilling. Indeed, these structures provide favorable zones for groundwater accumulation in the Ifni Inlier. The use of high-resolution electrical resistivity mapping (7200 Hz) in the study area confirmed the impact of faults on groundwater potential. This map showed that areas with fault crossings have low resistivity anomalies, indicating the presence of groundwater, while healthy basement formations have high resistivity ranges. This information is valuable for mapping and identifying potential groundwater zones, helping to identify geological faults that may influence groundwater availability. This study also illustrates the importance of using regional gravity data and high-resolution resistivity in structural analysis, particularly in areas where conventional geological mapping is hampered by a lack of outcrops due to recent sedimentary deposits.

Author Contributions: Conceptualization, M.I.; methodology, M.I. and M.J.; software, M.I., I.R. and F.Z.E.; validation, M.J., S.B., K.A., T.A.-A., A.K. and M.A.; formal analysis, M.I., A.K. and M.A.; investigation, M.I. and M.J.; resources, M.I.; data curation, M.I. and S.B.; writing—original draft preparation, M.I., M.J., I.R., F.Z.E., S.B., F.F. and A.K.; writing—review and editing, K.A., T.A.-A. and M.A.; visualization, M.I. and M.J.; supervision, S.B. and F.F.; project administration, M.A.; funding acquisition, K.A. All authors have read and agreed to the published version of the manuscript.

Funding: This research was funded by Researchers Supporting Project number (RSP2023R351), King Saud University, Riyadh, Saudi Arabia.

Institutional Review Board Statement: Not applicable.

Informed Consent Statement: Not applicable.

Data Availability Statement: The data presented in this study are available upon request from the corresponding author.

Conflicts of Interest: The authors declare no conflict of interest.

References

1. Kostyuchenko, Y.; Artemenko, I.; Abioui, M.; Benssaou, M. Global and Regional Climatic Modeling. In *Encyclopedia of Mathematical Geosciences*; Sagar, B.D., Cheng, Q., McKinley, J., Agterberg, F., Eds.; Springer: Cham, Switzerland, 2022; pp. 1–5. [CrossRef]
2. Schilling, J.; Freier, K.P.; Hertig, E.; Scheffran, J. Climate change, vulnerability and adaptation in North Africa with focus on Morocco. *Agric. Ecosyst. Environ.* **2012**, *156*, 12–26. [CrossRef]
3. Wang, Y.; Leung, L.R.; Mcgregor, J.L.; Lee, D.K.; Wang, W.C.; Ding, Y.; Kimura, F. Regional climate modeling: Progress, challenges, and prospects. *J. Meteorol. Soc. Jpn.* **2004**, *82*, 1599–1628. [CrossRef]
4. El Assaoui, N.; Sadok, A.; Merimi, I. Impacts of climate change on Moroccan's groundwater resources: State of art and development prospects. *Mater. Today Proc.* **2021**, *45*, 7690–7696. [CrossRef]
5. Benziane, F.; Yazidi, A.; Schulte, B.; Boger, S.; Stockhammer, S.; Lehmann, A.; Saadane, A.; Yazid, M. Notice Explicative Carte Géologique du Maroc au 1/50,000, Feuille Sidi Ifni. *Notes Mem. Serv. Géol. Maroc* **2016**, *542*.
6. Schulte, B.; Benziane, F.; Yazidi, A.; Boger, S.; Stockhammer, S.; Lehmann, A.; Saadane, A.; Yazidi, M. Notes Explicative Carte Géologique du Maroc au 1/50,000, Feuille Arbaa Sahel. *Notes Mém. Serv. Géol. Maroc* **2016**, *541*.
7. Yazidi, A.; Benziane, F.; Schulte, B.; Boger, S.; Stockhammer, S.; Lehmann, A.; Saadane, A.; Yazid, M. Notes Explicative Carte Géologique du Maroc au 1/50,000, Feuille Assaka. *Notes Mém. Serv. Géol. Maroc* **2016**, *544*.
8. Aude, J.L. Projet d'Accumulation Souterraine d'Eau en Massif Granitique (Oued Ifni-Maroc): Application de l'Analyse Structurale. Ph.D. Thesis, Université Scientifique et Médicale de Grenoble, Grenoble, France, 1983.
9. Khattach, D.; Keating, P.; Chennouf, T.; Andrieux, P.; Milhi, A. Apport de la gravimétrie à l'étude de la structure du bassin des Triffa (Maroc nord-oriental): Implications hydrogéologiques. *Comptes Rendus Geosci.* **2004**, *336*, 1427–1432. [CrossRef]
10. Najine, A.; Jaffal, M.; El Khammari, K.; Aifa, T.; Kattach, D.; Himi, M.; Casas, A.; Badrane, S.; Aqil, H. Contribution de la gravimétrie à l'étude de la structure du bassin de Tadla (Maroc): Implications hydrogéologiques. *C. R. Geosci.* **2006**, *338*, 676–682. [CrossRef]
11. El Goumi, N.; Jaffal, M.; Kchikach, A.; Manar, A. Apport de la gravimétrie à l'étude de la structure du bassin du Haouz (Maroc). *Estud. Geol.* **2010**, *66*, 181–191. [CrossRef]
12. Farhat, B.; Benassi, R.; Jallouli, C.; Ben Mammou, A. Contribution de la gravimétrie à l'étude de la structure de la plaine de Mornag (nord est de la Tunisie): Implications hydrogéologiques. *Hydrol. Sci. J.* **2010**, *55*, 1396–1404. [CrossRef]
13. Jaffal, M.; Charbaoui, A.; Kchikach, A.; El Ghorfi, M.; Khaldoun, A.; Safhi, A.E.M.; Bodinier, J.L.; Yazami, O.K.; Jourani, E.; Manar, A. Gravity study of the Western Bahira Basin and the Gantour Phosphatic Plateau, central Morocco: Interpretation and hydrogeological implications. *J. Afr. Earth Sci.* **2022**, *193*, 104581. [CrossRef]
14. Keating, P.; Pilkington, M.; Sailhac, P.; Nadeau, L. Locating Magnetic Contacts and Source Characteristics from Magnetic Data–Application to the Canadian Shield. In Proceedings of the 66th EAGE Conference& Exhibition, European Association of Geoscientists & Engineers, Paris, France, 7–10 June 2004.
15. Khazri, D.; Gabtni, H. New structural model to understanding the subsurface hydrogeology system of the Ouled Asker groundwater, Central Tunisian Atlasic foreland, derived from an integrated geophysical approach. *Arab. J. Geosci.* **2022**, *15*, 738. [CrossRef]
16. Everaerts, M.; Mansy, J.L. Le filtrage des anomalies gravimétriques; une clé pour la compréhension des structures tectoniques du Boulonnais et de l'Artois (France). *Bull. Soc. Géol. Fr.* **2001**, *172*, 267–274. [CrossRef]
17. Keating, P.; Pilkington, M. Euler deconvolution of the analytic signal and its application to magnetic interpretation. *Geophys. Prospect.* **2004**, *52*, 165–182. [CrossRef]
18. Zakariah, M.N.A.; Roslan, N.; Sulaiman, N.; Lee, S.C.H.; Hamzah, U.; Noh, K.A.M.; Lestari, W. Gravity analysis for subsurface characterization and depth estimation of Muda River Basin, Kedah, Peninsular Malaysia. *Appl. Sci.* **2021**, *11*, 6363. [CrossRef]
19. Jaffal, M.; El Goumi, N.; Kchikach, A.; Aïfa, T.; Khattach, D.; Manar, A. Gravity and magnetic investigations in the Haouz basin, Morocco. Interpretation and mining implications. *J. Afr. Earth Sci.* **2010**, *58*, 331–340. [CrossRef]
20. Amiri, A.; Chaqui, A.; Nasr, I.H.; Inoubli, M.H.; Ayed, N.B.; Tlig, S. Role of preexisting faults in the geodynamic evolution of Northern Tunisia, insights from gravity data from the Medjerda valley. *Tectonophysics* **2011**, *506*, 1–10. [CrossRef]
21. Melo, F.F.; Barbosa, V.C.; Uieda, L.; Oliveira, V.C.; Silva, J.B. Estimating the nature and the horizontal and vertical positions of 3D magnetic sources using Euler deconvolution A single Euler solution per anomaly. *Geophysics* **2013**, *78*, J87–J98. [CrossRef]
22. Ouerghi, S.; Rebai, N.; Gabtni, H.; Farhat, B.; Bouaziz, S. Apport de la gravimétrie à l'étude des structures effondrées du Nord-Est de la Tunisie: Implications hydrogéologiques. *Hydrol. Sci. J.* **2013**, *58*, 1361–1373. [CrossRef]
23. Dufréchou, G.; Harris, L.B. Tectonic models for the origin of regional transverse structures in the Grenville Province of SW Quebec interpreted from regional gravity. *J. Geodyn.* **2013**, *64*, 15–39. [CrossRef]
24. Aqil, H.; Khattach, D.; Gout, R.E.; Mandour, A.E.; Kaufmann, O. Contribution de la gravimétrie à l'étude de la structure profonde du bassin de Bou-Houria (Maroc Nord-oriental): Implications hydrogéologiques. *Hydrol. Sci. J.* **2015**, *60*, 736–745. [CrossRef]

25. Khattach, D.; Houari, M.R.; Corchete, V.; Chourak, M.; El Gout, R.; Ghazala, H. Main crustal discontinuities of Morocco derived from gravity data. *J. Geodyn.* **2013**, *68*, 37–48. [CrossRef]
26. Rezouki, I.; Boujamaoui, M.; Hafid, M.; Nait Bba, A.; Amiri, A.; Inoubli, M.H.; Manar, A.; Rouai, M.; Baidder, L.; Asebriy, L. Contribution of gravity and aeromagnetic data to the structural modeling of the hidden faults in Guercif Basin, northeastern Morocco. *J. Afr. Earth Sci.* **2020**, *164*, 103797. [CrossRef]
27. El Azzab, D.; Ghfir, Y.; Miftah, A. Geological interpretation of the rifian foreland gravity anomalies and 3D modeling of their Hercynian granites (Northeastern Morocco). *J. Afr. Earth Sci.* **2019**, *150*, 584–594. [CrossRef]
28. Ouchchen, M.; Boutaleb, S.; Abia, E.H.; El Azzab, D.; Abioui, M.; Mickus, K.L.; Miftah, A.; Echogdali, F.Z.; Dadi, B. Structural interpretation of the Igherm region (Western Anti Atlas, Morocco) from an aeromagnetic analysis: Implications for copper exploration. *J. Afr. Earth Sci.* **2021**, *176*, 104140. [CrossRef]
29. Cordell, L.; Grauch, V.J.S. Mapping Basement Magnetization Zones from Aeromagnetic Data in the San Juan Basin, New Mexico. In *The Utility of Regional Gravity and Magnetic Maps*; Hinze, W.J., Ed.; Society of Exploration Geophysicists: Tulsa, OK, USA, 1985; pp. 181–197. [CrossRef]
30. Cordell, L. Gravimetric expression of graben faulting in Santa Fe Country and the Espanola Basin. In *New Mexico Geological Society, Guidebook Conference*; New Mexico Geological Survey: Socorro, NM, USA, 1979.
31. Miller, H.G.; Singh, V. Potential field tilt-a new concept for location of potential field sources. *J. Appl. Geophys.* **1994**, *32*, 213–217. [CrossRef]
32. Salem, A.; Williams, S.; Fairhead, D.; Smith, R.; Ravat, D. Interpretation of magnetic data using tilt-angle derivatives. *Geophysics* **2008**, *73*, L1–L10. [CrossRef]
33. Fairhead, J.D.; Salem, A.; Cascone, L.; Hammill, M.; Masterton, S.; Samson, E. New developments of the magnetic tilt-depth method to improve structural mapping of sedimentary basins. *Geophys. Prospect.* **2011**, *59*, 1072–1086. [CrossRef]
34. Ravat, D. Analysis of the Euler method and its applicability in environmental magnetic investigations. *Environ. Eng. Geophys.* **1996**, *1*, 229–238. [CrossRef]
35. Gabtni, H.; Jallouli, C.; Mickus, K.L.; Turki, M.M. Geodynamics of the Southern Tethyan Margin in Tunisia and Maghrebian domain: New constraints from integrated geophysical study. *Arab. J. Geosci.* **2013**, *6*, 271–286. [CrossRef]
36. Arfaoui, M.; Reid, A.; Inoubli, M.H. Evidence for a new regional NW–SE fault and crustal structure in Tunisia derived from gravity data. *Geophys. Prospect.* **2015**, *63*, 1272–1283. [CrossRef]
37. Ikirri, M.; Faik, F.; Boutaleb, S.; Echogdali, F.Z.; Abioui, M.; Al-Ansari, N. Application of HEC–RAS/WMS and FHI models for the extreme hydrological events under climate change in the Ifni River arid watershed from Morocco. In *Climate and Land Use Impacts on Natural and Artificial Systems: Mitigation and Adaptation*; Nistor, M.M., Ed.; Elsevier: Amsterdam, The Netherlands, 2021; pp. 251–270. [CrossRef]
38. Ikirri, M.; Faik, F.; Echogdali, F.Z.; Antunes, I.M.H.R.; Abioui, M.; Abdelrahman, K.; Fnais, M.S.; Wanaim, A.; Id-Belqas, M.; Boutaleb, S.; et al. Flood Hazard Index Application in Arid Catchments: Case of the Taguenit Wadi Watershed, Lakhssas, Morocco. *Land* **2022**, *11*, 1178. [CrossRef]
39. Hollard, H.; Choubert, G.; Bronner, G.; Marchand, J.; Sougy, J. Carte Géologique du Maroc, scale 1/1000000 (2 sheets). In *Notes et Mémoires du Service Géologique du Maroc*; Service Géologique du Maroc: Rabat, Morocco, 1985; 260p.
40. Soulaimani, A.; Michard, A.; Ouanaimi, H.; Baidder, L.; Raddi, Y.; Saddiqi, O.; Rjimati, E.C. Late Ediacaran–Cambrian structures and their reactivation during the Variscan and Alpine cycles in the Anti-Atlas (Morocco). *J. Afr. Earth Sci.* **2014**, *98*, 94–112. [CrossRef]
41. Jeannette, D.; Benziane, F.; Yazidi, A. Lithostratigraphie et datation du Protérozoïque de la boutonnière d'Ifni (Anti-Atlas, Maroc). *Precambrian Res.* **1981**, *14*, 363–378. [CrossRef]
42. Thomas, R.J.; Fekkak, A.; Ennih, N.; Errami, E.; Loughlin, S.C.; Gresse, P.G.; Chevallier, L.P.; Liégeois, J.P. A new lithostratigraphic framework for the Anti-Atlas Orogen, Morocco. *J. Afr. Earth Sci.* **2004**, *39*, 217–226. [CrossRef]
43. Mortaji, A.; Gasquet, D.; Ikenne, M.; Beraaouz, E.H.; Barbey, P.; Lahmam, M.; El Aouli, E.H. Les granitoïdes tardi-panafricains de l'Anti-Atlas sud-occidental (Maroc): Evolution d'un type magnésien à un type ferrifère. Exemple de la boutonnière d'Ifni. *Estud. Geol.* **2007**, *63*, 7–25. [CrossRef]
44. Charton, R.; Bertotti, G.; Arantegui, A.; Bulot, L. The Sidi Ifni transect across the rifted margin of Morocco (Central Atlantic): Vertical movements constrained by low-temperature thermochronology. *J. Afr. Earth Sci.* **2018**, *141*, 22–32. [CrossRef]
45. Yazidi, A. Les Formations Sédimentaires et Volcaniques de la Boutonnière d'Ifni, Maroc. Ph.D. Thesis, Université Scientifique et Médicale de Grenoble, Grenoble, France, 1976.
46. Benziane, F. Géologie de la Boutonnière précambrienne d'Ifni (Anti-Atlas occidental). In *Editions du Service Géologique du Maroc*; Service Géologique du Maroc: Rabat, Morocco, 1982; 312p.
47. Sebbab, M.M.; El Ouahidi, A.; Ousbih, M.; Ouboulahcen, S.; Abdelrahman, K.; Abioui, M. Integrated Geotechnical Approach and GIS for Identification of Geological Resources Exploitable Quarries for Sustainable Development in Ifni Inlier and Lakhssas Plateau (Western Anti Atlas, Morocco). *Appl. Sci.* **2023**, *13*, 3932. [CrossRef]
48. Sdzuy, K. The Precambrian–Cambrian boundary beds in Morocco (preliminary report). *Geol. Mag.* **1978**, *115*, 83–94. [CrossRef]
49. Benssaou, M.; M'Barki, L.; Ezaidi, A.; Abioui, M. Geodynamic significance of studying Lower Cambrian Sequence units in the western Anti-Atlas. *Int. J. Mater. Sci. Appl.* **2017**, *6*, 142–147. [CrossRef]

50. Ikirri, M.; Boutaleb, S.; Ibraheem, I.M.; Abioui, M.; Echogdali, F.Z.; Abdelrahman, K.; Id-Belqas, M.; Abu-Alam, T.; El Ayady, H.; Essoussi, S.; et al. Delineation of Groundwater Potential Area using an AHP, Remote Sensing, and GIS Techniques in the Ifni Basin, Western Anti-Atlas, Morocco. *Water* **2023**, *15*, 1436. [CrossRef]
51. Silva-Ávalos, R.U.; Júnez-Ferreira, H.E.; González-Trinidad, J.; Bautista-Capetillo, C. Non-Linear 3D Satellite Gravity Inversion for Depth to the Basement Estimation in a Mexican Semi-Arid Agricultural Region. *Appl. Sci.* **2022**, *12*, 7252. [CrossRef]
52. Van Den Bosch, J.W.D. Carte gravimétrique du Maroc (Provinces du Nord) au 1/500,000. *Notes Mém. Serv. Géol. Maroc* **1981**, *234*.
53. Gérard, A.; Griveau, P. Interprétation quantitative en gravimétrie ou magnétisme à partir de cartes transformées de gradient vertical. *Geophys. Prospect.* **1972**, *20*, 459–481. [CrossRef]
54. Fitz Gerald, D.; Reid, A.; McInerney, P. New discrimination techniques for Euler deconvolution. In Proceedings of the 8th SAGA Biennial Technical Meeting and Exhibition EAGE, Pilanesberg, South Africa, 7–10 October 2003.
55. Vanié, L.T.A.; Khattach, D.; Houari, M. Apport des filtrages des anomalies gravimétriques à l'étude des structures profondes du Maroc oriental. *Bull. Inst. Sci.* **2005**, *27*, 29–40.
56. Khattach, D.; Mraoui, H.; Sbibih, D.; Chennouf, T. Analyse multi-échelle par ondelettes des contacts géologiques: Application à la carte gravimétrique du Maroc nord-oriental. *Comptes Rendus Geosci.* **2006**, *338*, 521–526. [CrossRef]
57. Martelet, G.; Perrin, J.; Truffert, C.; Deparis, J. Fast mapping of magnetic basement depth, structure and nature using aeromagnetic and gravity data: Combined methods and their application in the Paris Basin. *Geophys. Prospect.* **2013**, *61*, 857–873. [CrossRef]
58. Nait Bba, N.; Boujamaoui, M.; Amiri, A.; Hejja, Y.; Rezouki, I.; Baidder, L.; Inoubli, M.H.; Manar, A.; Jabour, H. Structural modeling of the hidden parts of a Paleozoic belt: Insights from gravity and aeromagnetic data (Tadla Basin and Phosphates Plateau, Morocco). *J. Afr. Earth Sci.* **2019**, *151*, 506–522. [CrossRef]
59. Elabouyi, M.; Yaagoub, D.; Driouch, Y.; Dahire, M.; Qarqori, K.; Manar, A.; Ntarmouchant, A.; Laguenini, F.; Malic, B.; Jeddi, M.; et al. The buried Variscan granites and associated structures in the High Moulouya basin from gravity data and their role during the Triassic-Liassic extensional tectonics (Moroccan Meseta-Atlas domain). *J. Afr. Earth Sci.* **2022**, *193*, 104597. [CrossRef]
60. Bouiflane, M. Cartographies Aéromagnétique et Magnétique Multi-Echelles: Étude Structurale d'une Région du Fossé Rhénan. Ph.D. Thesis, Université Louis Pasteur, Strasbourg, France, 2008.
61. Blakely, R.J.; Simpson, R.W. Approximating edges of source bodies from magnetic or gravity anomalies. *Geophysics* **1986**, *51*, 1494–1498. [CrossRef]
62. Grauch, V.J.S.; Cordell, L. Limitations of determining density or magnetic boundaries from the horizontal gradient of gravity or pseudogravity data. *Geophysics* **1987**, *52*, 118–121. [CrossRef]
63. Marson, I.; Klingele, E.E. Advantages of using the vertical gradient of gravity for 3-D interpretation. *Geophysics* **1993**, *58*, 1588–1595. [CrossRef]
64. Reid, A.B.; Allsop, J.M.; Granser, H.; Millett, A.J.; Somerton, I.W. Magnetic interpretation in three dimensions using Euler deconvolution. *Geophysics* **1990**, *55*, 80–91. [CrossRef]
65. Verduzco, B.; Fairhead, J.D.; Green, C.M.; MacKenzie, C. New insights into magnetic derivatives for structural mapping. *Lead. Edge* **2004**, *23*, 116–119. [CrossRef]
66. Thompson, D.T. EULDPH: A new technique for making computer-assisted depth estimates from magnetic data. *Geophysics* **1982**, *47*, 31–37. [CrossRef]
67. Cooper, G.R.J. The automatic determination of the location and depth of contacts and dykes from aeromagnetic data. *Pure Appl. Geophys.* **2014**, *171*, 2417–2423. [CrossRef]
68. Barbosa, V.C.F.; Silva, J.B.C.; Medeiros, W.E. Stability analysis and improvement of structural index estimation in Euler deconvolution. *Geophysics* **1999**, *64*, 48–60. [CrossRef]
69. Barbosa, V.C.; Silva, J.B. Reconstruction of geologic bodies in depth associated with a sedimentary basin using gravity and magnetic data. *Geophys. Prospect.* **2011**, *59*, 1021–1034. [CrossRef]
70. Ugalde, H.; Morris, W.A. Cluster analysis of Euler deconvolution solutions: New filtering techniques and geologic strike determination. *Geophysics* **2010**, *75*, L61–L70. [CrossRef]
71. Amar, M.; Manar, A.; Boualoul, M. Apport de la cartographie aéromagnétique à l'identification structurale du système aquifère des sources de l'oasis de Figuig (Maroc). *Bull. Inst. Sci.* **2012**, *34*, 29–40.
72. Draper, N.R.; Smith, H. *Applied Regression Analysis*, 3rd ed.; John Wiley& Sons: Hoboken, NJ, USA, 1998.
73. Das, S. Comparison among influencing factor, frequency ratio, and analytical hierarchy process techniques for groundwater potential zonation in Vaitarna basin, Maharashtra, India. *Groundw. Sustain. Dev.* **2019**, *8*, 617–629. [CrossRef]
74. Mukherjee, I.; Singh, U.K. Delineation of groundwater potential zones in a drought-prone semi-arid region of east India using GIS and analytical hierarchical process techniques. *Catena* **2020**, *194*, 104681. [CrossRef]
75. Andualem, T.G.; Demeke, G.G. Groundwater potential assessment using GIS and remote sensing: A case study of Guna tank landscape, upper Blue Nile Basin, Ethiopia. *J. Hydrol. Reg. Stud.* **2019**, *24*, 100610. [CrossRef]
76. Echogdali, F.Z.; Boutaleb, S.; Kpan, R.B.; Ouchchen, M.; Bendarma, A.; El Ayady, H.; Abdelrahman, K.; Fnais, S.M.; Sajinkumar, K.S.; Abioui, M. Application of fuzzy logic and fractal modeling approach for groundwater potential mapping in semi-arid Akka basin, Southeast Morocco. *Sustainability* **2022**, *14*, 10205. [CrossRef]
77. Razandi, Y.; Pourghasemi, H.R.; Neisani, N.S.; Rahmati, O. Application of analytical hierarchy process, frequency ratio, and certainty factor models for groundwater potential mapping using GIS. *Earth Sci. Inform.* **2015**, *8*, 867–883. [CrossRef]

78. Abijith, D.; Saravanan, S.; Singh, L.; Jennifer, J.J.; Saranya, T.; Parthasarathy, K.S.S. GIS-based multi-criteria analysis for identification of potential groundwater recharge zones–a case study from Ponnaniyaru watershed, Tamil Nadu, India. *HydroResearch* **2020**, *3*, 1–14. [CrossRef]
79. Delorme, M. Ecoulements en Milieux Fracturés: Vers une Intégration des Approches Discrètes et Continues. Ph.D. Thesis, Université de Toulouse, Toulouse, France, 2015.
80. Yousefi, M.; Carranza, E.J.M. Geometric average of spatial evidence data layers: A GIS-based multi-criteria decision making approach to mineral prospectivity mapping. *Comput. Geosci.* **2015**, *83*, 72–79. [CrossRef]
81. Yousefi, M.; Nykänen, V. Data-driven logistic-based weighting of geochemical and geological evidence layers in mineral prospectivity mapping. *J. Geochem. Explor.* **2016**, *164*, 94–106. [CrossRef]
82. Echogdali, F.Z.; Boutaleb, S.; Abia, E.H.; Ouchchen, M.; Dadi, B.; Id-Belqas, M.; Abioui, M.; Pham, L.T.; Abu-Alam, T.; Mickus, K.L. Mineral prospectivity mapping: A potential technique for sustainable mineral exploration and mining activities—A case study using the copper deposits of the Tagmout basin, Morocco. *Geocarto Int.* **2022**, *37*, 9110–9131. [CrossRef]
83. Yousefi, M.; Kamkar-Rouhani, A.; Carranza, E.J.M. Application of staged factor analysis and logistic function to create a fuzzy stream sediment geochemical evidence layer for mineral prospectivity mapping. *Geochem. Explor. Environ. Anal.* **2014**, *14*, 45–58. [CrossRef]
84. Yousefi, M.; Carranza, E.J.M. Prediction–area (P–A) plot and C–A fractal analysis to classify and evaluate evidential maps for mineral prospectivity modeling. *Comput. Geosci.* **2015**, *79*, 69–81. [CrossRef]
85. Alzahrani, H.; Abdelrahman, K.; Hazaea, S.A. Use of geoelectrical resistivity method for detecting near-surface groundwater potential zones at Riyadh city, Saudi Arabia. *J. King Saud Univ. Sci.* **2022**, *34*, 102253. [CrossRef]
86. Alarifi, S.S.; Abdelrahman, K.; Hazaea, B.Y. Near-surface groundwater exploration using the geoelectrical resistivity method: A case study of Wadi Nisah, Riyadh, Saudi Arabia. *J. King Saud Univ. Sci.* **2022**, *34*, 102207. [CrossRef]
87. Jamal, N.; Singh, N.P. Identification of fracture zones for groundwater exploration using very low frequency electromagnetic (VLF-EM) and electrical resistivity (ER) methods in hard rock area of Sangod Block, Kota District, Rajasthan, India. *Groundw. Sustain. Dev.* **2018**, *7*, 195–203. [CrossRef]
88. Meju, M.A. Simple effective resistivity-depth transformations for infield or real-time data processing. *Comput. Geosci.* **1995**, *21*, 985–992. [CrossRef]
89. Bittar, M.S.; Rodney, P.F.; Mack, S.G.; Bartel, R.P. A multiple-depth-of-investigation electromagnetic wave resistivity sensor: Theory, experiment, and field test results. *SPE Form. Eval.* **1993**, *8*, 171–176. [CrossRef]
90. Siemon, B. Improved and new resistivity-depth profiles for helicopter electromagnetic data. *J. Appl. Geophys.* **2001**, *46*, 65–76. [CrossRef]
91. Huang, H. Depth of investigation for small broadband electromagnetic sensors. *Geophysics* **2005**, *70*, G135–G142. [CrossRef]
92. Li, H.; Wang, H. Investigation of eccentricity effects and depth of investigation of azimuthal resistivity LWD tools using 3D finite difference method. *J. Pet. Sci. Eng.* **2016**, *143*, 211–225. [CrossRef]
93. Simpson, R.W.; Jachens, R.C.; Blakely, R.J.; Saltus, R.W. A new isostatic residual gravity map of the conterminous United States with a discussion on the significance of isostatic residual anomalies. *J. Geophys. Res. Solid Earth* **1986**, *91*, 8348–8372. [CrossRef]
94. Walter, B. Réservoirs de Socle en Contexte Extensif: Genèse, Géométries et Circulations de Fluides: Exemples du Rift Intracontinental du Lac Albert (Ouganda) et de la Marge Proximale d'Ifni (Maroc). Ph.D. Thesis, Université de Lorraine, Lorraine, France, 2016.
95. Yazidi, A.; Benziane, F.; Hollard, H.; Oliva, P.; Destombes, J. Carte Géologique du Maroc et notice: Sidi Ifni, scale 1/100000. *Notes Mém. Serv. Géol. Maroc* **1986**, *310*.